Evaluating the Influence of Rotor-Casing Eccentricity on Turbine Efficiency Including Time-Resolved Flow Field Measurements

Eric T. DeShong[1]
Department of Mechanical Engineering,
Pennsylvania State University,
3127 Research Drive, Rm 144,
State College, PA 16801
e-mail: etd5060@psu.edu

Shawn Siroka
Department of Mechanical Engineering,
Pennsylvania State University,
3127 Research Drive, Rm 164,
State College, PA 16801
e-mail: sis5702@psu.edu

Reid A. Berdanier
Department of Mechanical Engineering,
Pennsylvania State University,
3127 Research Drive, Rm 147,
State College, PA 16801
e-mail: rberdanier@psu.edu

Karen A. Thole
Department of Mechanical Engineering,
Pennsylvania State University,
3127 Research Drive, Rm 148,
State College, PA 16801
e-mail: kthole@engr.psu.edu

The clearance that exists between the casing and turbine blade tips is one of the key drivers of efficiency in gas turbine engines. For this reason, engine manufacturers utilize precise manufacturing techniques and may use clearance control systems to minimize tip clearances to reduce associated losses. Despite these efforts, turbines typically exhibit some nominal casing ovality or rotor-casing eccentricity, and changes to blade tip clearance during operation commonly occur due to thermal and mechanical stresses. The present study investigates non-axisymmetric tip clearance effects by creating a rotor-casing eccentricity in a one-stage axial test turbine operating in a continuous-duration mode at engine-relevant conditions with engine representative hardware. A magnetic levitation bearing system was leveraged to move the turbine shaft to vary the rotor-casing eccentricity without test section disassembly. The results of this study indicate that rotor-casing eccentricity does not affect overall turbine efficiency over the range that was tested, but does locally influence efficiency and the rotor exit flow field. Comparisons of flow angle and secondary flow kinetic energy (SKE) agreed with previous studies and existing analytical methods, respectively. Collectively, these results indicate that tip clearance can be studied locally on an eccentric rotor. [DOI: 10.1115/1.4052318]

Keywords: cavity and leaking flows, and turbine aerodynamic design, fluid dynamics and heat transfer phenomena in compressor and turbine components of gas turbine engines

Introduction

The power generation and aviation industries rely heavily on gas turbine technology due to its efficiency and reliability. Global energy production from gas turbine engines is projected to double between 2014 and 2024 [1], and the commercial aircraft market is expected to grow by 64 billion dollars between 2018 and 2028 [2]. Therefore, it is important to develop a thorough understanding of the factors that contribute to engine efficiency and durability, which will improve engine reliability and further reduce the environmental impact from harmful gas emissions.

The flow through the turbine blade tip gap that exists between the rotating blades, and the stationary casing has a large impact on turbine efficiency. In practice, many thermal and mechanical stresses associated with engine operation can cause blade tip clearance variations. A key driver of turbine efficiency is the clearance that exists between the rotating blade tips and the stationary casing wall. The pressure difference across the blade tip drives a flow through the clearance gap, and there is a contributing viscous effect due to the motion of the endwall relative to the blade tips. As the blade tip gap increases, the additional flow through the gap increases loss generation and decreases energy extraction. Bunker [3] estimated this impact by explaining that up to a 2:1 ratio exists between turbine efficiency and tip clearance relative to blade span. Because of this effect, engine manufacturers strive to minimize the tip clearance using precise manufacturing techniques and clearance control systems [4]. Despite these efforts, blade tip clearance commonly changes during routine operation.

Changes to the blade tip clearance can be axisymmetric or non-axisymmetric based on the nature of the fault that causes the change. In the axisymmetric case, the tip clearance is constant around the entire annulus. In the non-axisymmetric case, the tip clearance changes around the annulus due to rotor shaft or casing deflection. As an example of non-axisymmetric variations, casing out-of-roundness can occur when a temperature gradient forms in the turbine case or shroud. Furthermore, casing deflection commonly occurs in aviation engines during changes of aerodynamic and thrust loads. This casing deflection occurs because engines are not mounted at their centerline, which causes a torque about the mounting location [4]. Bunker [3] identified nominal casing out-of-roundness as a major factor that must be accounted for when designing turbine blade tips. This nominal ovality is evidenced, in part, by localized tip rub events, which Bunker noted are common in practice. These faults experienced during standard engine operation are imposed in addition to any geometric variations that may have occurred during engine component manufacturing.

Literature Review

Only a small collection of studies have examined the effects of non-axisymmetric tip clearance in turbomachinery. The majority of these studies have focused on assessing the effect of eccentricity, which creates a non-axisymmetric blade tip clearance, on rotordynamic instabilities [5–9]. These studies allude to a tip clearance driven performance variation around the annulus, but do not directly investigate it. Guo et al. [10] and Guo and Rhode [11] investigated the effects of rotor-casing eccentricity on the

[1]Corresponding author.

Contributed by the International Gas Turbine Institute (IGTI) of ASME for publication in the Journal of Turbomachinery. Manuscript received July 16, 2021; final manuscript received August 23, 2021; published online October 1, 2021. Tech. Editor: David G. Bogard.

performance of turbine rim seals with purge flow injection and identified a considerable decrease of rim sealing effectiveness with the introduction of eccentricity.

Although research on non-axisymmetric clearances has been limited, there is a relatively large body of literature examining axisymmetric tip clearance effects. The results of these studies can be used to develop a fundamental understanding of the loss mechanisms created by a non-axisymmetric tip clearance. Many researchers have used cascade facilities to investigate the tip clearance flows, but without the complexities caused by rotational effects. For example, Bindon [12] studied the tip leakage vortex (TLV), which forms as the leakage flow passes over the blade tip from pressure side to suction side and interacts with the main passage flow. Peters and Moore [13] showed the mixing process that occurs between the tip leakage flow and the mainstream flow causes associated losses that reach about 85% of their maximum value at 40% of the axial chord length downstream of the blade trailing edge. Yaras et al. [14] used a similar experimental setup to study the downstream losses for three different tip clearances, and these authors concluded that the mixing process occurs very rapidly downstream of the blade row. In general, the kinetic energy (KE) of the tip leakage flow is a key indicator of turbine stage performance debits [15]. Although these cascade studies are necessary for building an understanding of the sources of loss in a turbine stage, an extension to rotating test facilities includes additional factors that may be missed in cascade experiments, such as the motion of the endwall relative to the blades.

Rotating test rigs further build upon the understanding of tip leakage flows by incorporating the effect that rotation has on the flow field. Morphis and Bindon [16] used a 1.5 stage turbine to examine performance as a function of tip clearance and tip gap geometry. They observed a 2% debit to efficiency when tip clearance increased by 1.5% of the blade span. Furthermore, the authors suggested a nonlinear relationship between tip clearance and efficiency based on three measured clearances. Yoon et al. [17] compared the performance of shrouded and unshrouded turbine blade tips using a 1.5 stage rotating test rig. In the case of unshrouded blades, calculated efficiency decreased nearly linear with increasing tip clearance. Their results compared well with the linear correlation also proposed by Hong and Groh [18]. Ameri et al. [19] used RANS simulations to assess flow through a blade row with a recessed tip gap to show a linearly decreasing trend of efficiency with increasing blade tip clearance. Results from this simulation indicated a 5% efficiency loss caused by a 3% increase in blade span relative tip clearance.

Based on this collection of results, it is expected that the general relationship between efficiency and tip clearance is approximately linear, which is further supported by various correlations established experimentally [20–24]. These correlations use a combination of blade geometry, drag coefficient, flow, and reaction to predict the efficiency detriment due to changes in tip clearance [25]. Furthermore, the ratio of efficiency loss to blade span relative tip clearance increase is typically between 1:1 and 2:1. The variation of this relationship between clearance and efficiency (also referred to as the efficiency gradient) is in part due to differences in blade loading, as evidenced in the correlation dependence presented by Lakshminarayana [23].

When a linear assumption is applied to a non-axisymmetric tip clearance caused by a rotor-casing eccentricity, it is expected that the efficiency increase in the small clearance region will be directly balanced by the efficiency decrease in the large clearance region. In turn, the resulting overall efficiency will be unchanged with respect to a concentric case with the same average tip clearance. However, to understand the physical mechanisms that affect efficiency, it is necessary to examine the flow features that cause loss.

Lakshminarayana created and validated a theoretical model of a tip leakage vortex with solid body rotation to predict the effect of clearance on secondary kinetic energy and outlet flow angle [23]. Gaetani et al. [26] used relative blade outlet flow angle measurements to identify the rotating flow structures corresponding to the TLV, tip passage vortex (TPV), and hub passage vortex (HPV) at the exit of a high pressure turbine stage using a fast-response aerodynamic probe (FRAP) positioned downstream of the rotor. A migration of the TPV and HPV toward the midspan was observed, which was attributed to the high flow turning, low blade aspect ratio, large circumferential width of the TLV, and rotational effects. Similarly, Behr et al. [27] used absolute flow yaw angle to identify adjacent flow overturning and underturning, which is characteristic of a vortex.

While the effects of tip clearance on turbine performance and flow field have been well studied, the exact application of these findings to the case of a non-axisymmetric blade tip clearance is unclear. To address this gap in understanding, the present study assesses the effects of rotor-casing eccentricity on turbine efficiency and rotor exit flow field. This study is unique because of the ability to use a magnetic bearing to precisely position the turbine shaft while using actual engine hardware.

Experimental Methods

Test Facility. This study was conducted at the Steady Thermal Aero Research Turbine (START) Lab at the Pennsylvania State University. A detailed explanation was given by Barringer et al. [28] and an abbreviated summary is given here. The START lab operates in an open-loop continuous-duration mode using two 1.1 MW (1500 hp) industrial compressors to supply the test section with a total flowrate of up to 11.4 kg/s (25 lb_m/s) at approximately 480 kPa (70 psia). Flow exits the compressors at a nominal temperature of 380 K (230 °F) and enters an in-line natural gas heater with capability to increase the temperature of the flow up to a maximum of 675 K (750 °F). Separately, pressurized air can be supplied to several independently metered cooling flows which are distributed to different locations in the turbine test section. The rotor speed is controlled to within ±10 rpm of a given set point by a water brake dynamometer, which can extract up to 895 kW (1200 hp) of power at a maximum rotating speed of 11,000 rpm. Finally, the pressure ratio across the turbine test section is adjusted using a valve downstream of the test section. Figure 1 shows a layout of the facility.

The test section consists of a single stage turbine (vane and blade) that operates at engine representative rotational and blade inlet Reynolds numbers, as introduced by Berdanier et al. [29]. As previously explained by Barringer et al. [28], the START rotor assembly is supported by magnetic levitation bearings during operation. This magnetic bearing system enables rapid iteration through varying amounts of rotor-casing eccentricity by imposing radial movements on the rotor assembly. Initially, these rotor movements were measured using four tip clearance probes to provide a baseline understanding of rotor position as magnetic bearing movements were introduced. An example of these movements is provided in Fig. 2, which shows tip clearance probe measurements gathered

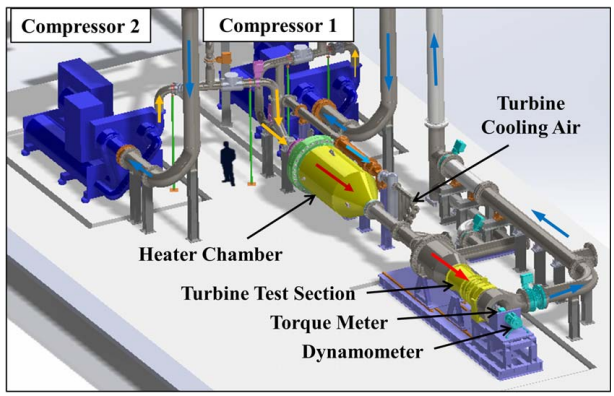

Fig. 1 PSU-START research facility system layout

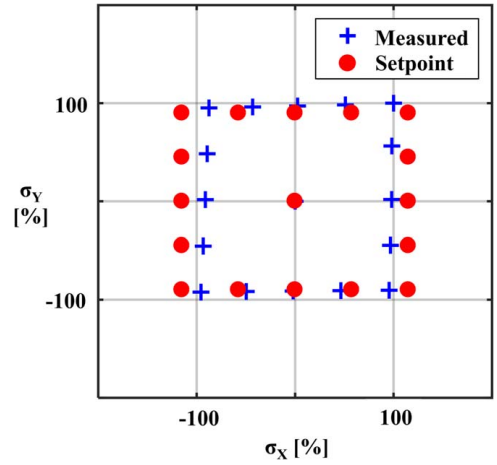

Fig. 2 Rotor centroid movements set by magnetic bearing (dots) and measured by tip clearance probes (crosses)

during a benchmarking experiment designed to verify the magnetic bearing and tip clearance probe capabilities. In Fig. 2, the tip clearance changes are presented using a normalized clearance variation, σ, defined by Eq. (1)

$$\sigma = \frac{\tau - \tau_0}{\tau_{\max} - \tau_0} \times 100\,(\%) \tag{1}$$

where τ represents the measured clearance from a given probe, τ_0 represents the nominal concentric clearance, and $\tau_{\max}$ represents the maximum tip clearance across all cases.

After completing this baseline assessment, two tip clearance sensors were removed and replaced with different sensors to collect data for a separate study (not presented here). With knowledge of the tip clearance in two positions, it is possible to relate the annular position to the local tip clearance. This process is shown in Fig. 3 for each eccentricity case. The eccentricity, ε, is calculated using Eq. (2)

$$\varepsilon = \sigma_{\mathrm{FRAP}} = \frac{\tau_{\mathrm{FRAP}} - \tau_0}{\tau_{\max} - \tau_0} \times 100\,(\%) \tag{2}$$

where σ_{FRAP} is the nondimensional tip clearance evaluated at the circumferential location of the FRAP. The FRAP was used to measure the flowfield downstream of the blades and will be further described in the Instrumentation section.

This process assumes a near-perfect circularity of the casing. Although tip clearance and hardware inspections showed no measurable out-of-roundness of the casing, it is important to note that

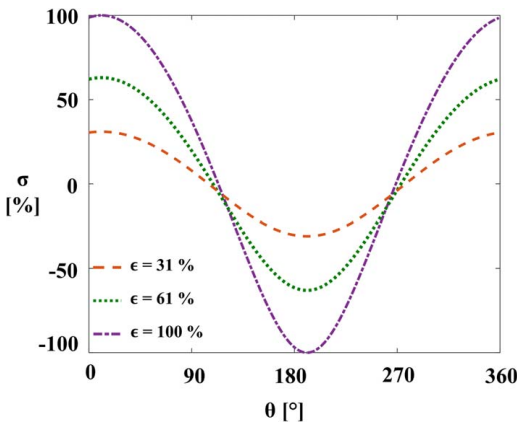

Fig. 3 Mapping of circumferential position to relative tip clearance change for all eccentricity cases

there still may be local manufacturing irregularities which directly affect the mapping between circumferential position and tip clearance. However, it should be noted that introducing any unexpected small out-of-roundness to these calculations has a negligible impact on the interpretations presented in this study.

Instrumentation. A collection of time-averaged and time-resolved measurement systems were implemented together to gather the results for this study. The layout of these measurements is shown in Fig. 4. The main gas path (MGP) and coolant flowrates were measured using Venturi flowmeters upstream of the test section. The turbine inlet total pressure and temperature were each gathered using six probes equally distributed circumferentially at the midspan of the inlet plane (P1). The coolant inlet total pressure and temperature were measured as the flow entered the internal passages of the test section. Together, these flowrates, pressures, and temperatures define the initial states of the MGP and coolant flows.

The outlet total pressure and temperature were measured at plane P2, which was located approximately three axial chord lengths downstream of the blade trailing edge. At plane P2, circumferential traverses of multi-element pressure and temperature rakes (each containing 10 radially distributed Kiels) define the turbine exit conditions. Due to hardware restrictions, several sections of the annulus were inaccessible for rake traverse measurements during this study. The motion of the rake traverses and the approximate positions of the inaccessible traverse locations are shown in Fig. 5 with relative relationship to the over-rotor and rotor exit measurement systems.

The rotor tip clearance data were measured by capacitive tip clearance probes located in the positions shown in Fig. 5, as described by Berdanier et al. [29]. Although individual blade clearance data were resolved for these tests, reported data represent averages of all blades over approximately 300 revolutions of steady operation. These tip clearance measurements were used to precisely quantify the local tip clearance changes at the FRAP mounting position, which enables the connection between tip clearance and flow feature variations.

A fast responding aerodynamic probe (FRAP) was used to measure time-resolved flow features exiting the turbine rotor. The details of the FRAP used in this experiment were given in detail by Pfau et al. [30], and a brief summary is provided here.

Fast responding aerodynamic probe measurement technology uses fast-response pressure transducers and applies potential flow theory to relate the pressure distribution across the probe head to the local flow velocity. The FRAP used in these experiments applied two pressure sensors in a virtual four-sensor operation mode to measure all three components of velocity. The mean flow angle at the FRAP measurement plane was first measured using a pneumatic three-hole probe. The FRAP was then yawed about this mean flow direction to ensure the FRAP was operated within its calibration range.

Due to the high temporal resolution of the FRAP, it is necessary to quantify the dynamic response of the measurement system. The manufacturer defined a 25 kHz cutoff frequency at 3 dB, characterized by acoustic excitations by a high velocity jet. For tests in the

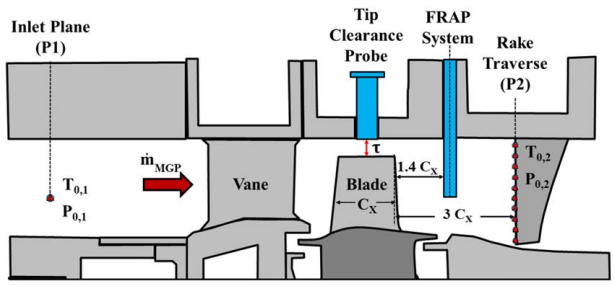

Fig. 4 Turbine cross section and instrumentation layout

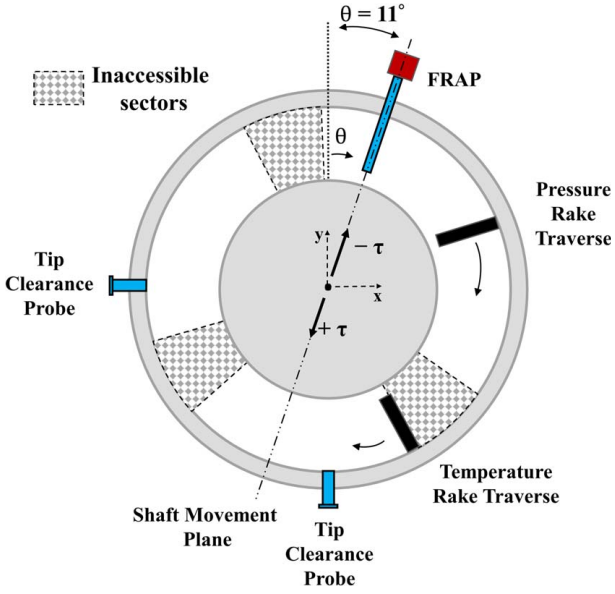

Fig. 5 Test section outlet and over-rotor instrumentation locations

START facility, time-resolved FRAP signals were further examined for spurious frequency peaks corresponding to vortex shedding or probe vibrations, but no features were identified. Based on this examination, a digital filter was applied at 25 kHz. This full-probe bandwidth resolves the fundamental and next two harmonics of the blade passing frequency, which is sufficient to resolve the unsteady fluctuations in the flow [31].

In this study, the FRAP was specifically used to quantify total pressure coefficient, flow yaw angle, and secondary flow kinetic energy (SKE) downstream of the rotor as a function of local blade tip clearance. The yaw angle is defined according to the convention shown in Fig. 6 in the stationary frame of reference. The SKE is calculated by first defining the primary flow direction as the circumferentially averaged flow direction at the midspan. Because the midspan region contains the highest mass flux and it is least affected by secondary flows, this definition of the primary flow direction gives a good approximation of the bulk fluid motion against which secondary flows will mix and create aerodynamic losses. The primary flow vector was computed for each case individually to ensure that any case-to-case variation in the bulk fluid flow direction does not contribute to the calculation of SKE.

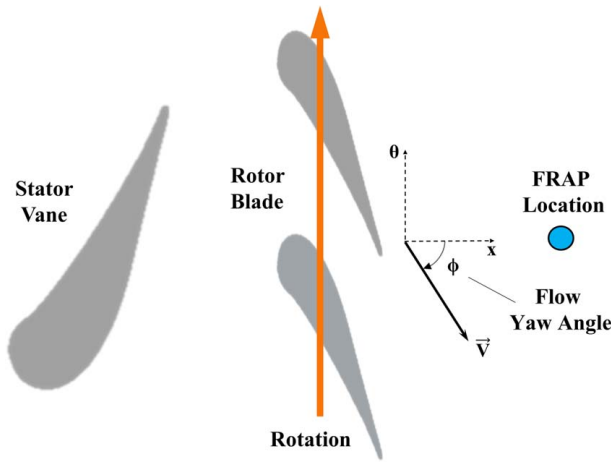

Fig. 6 Airfoil orientation, rotor rotation direction, and flow angle definition

The secondary flow vectors are then defined as the component of the ensemble-averaged velocity vectors perpendicular to the main flow vector. Finally, the SKE is calculated at all radial and temporal instances using the secondary flow vectors.

The uncertainty of these FRAP measurements was estimated by the system manufacturer. It is worth noting that the flow yaw angle uncertainty accounts for the mounting angle uncertainty in addition to the manufacturer estimated uncertainty. The mounting angle uncertainty is a result of the manual alignment of the FRAP to the centerline direction of the turbine, which was done using a point laser. The random uncertainty of the flow yaw angle measurement excludes the mounting angle uncertainty and is equivalent to 0.05 deg. These representative uncertainty values are shown in Table 1 alongside estimated uncertainties of the other measurement systems used in this study. The flowrate, pressure, temperature, and tip clearance uncertainties were calculated by Berdanier et al. [29], who followed the method outlined by Figliola and Beasley [32].

Testing Procedure. Initially, the rotor shaft was placed in the concentric position using the magnetic bearing. After reaching a thermally soaked steady-state operating condition for the turbine, circumferential exit rake traverses and radial FRAP traverses were performed at the concentric condition to define the nominal efficiency and rotor exit flow field, respectively. Radial rotor movements were then imposed along the movement plane indicated in Fig. 5. The trigonometric relationships between the FRAP position and the tip clearance probes were used to relate the magnetic bearing rotor movement inputs (X,Y) to the expected tip clearance changes at the tip clearance probe mounting positions.

In total, FRAP traverses were completed for 14 different eccentricity conditions. Eccentricity points within the local tip clearance measurement uncertainty range were averaged together, which resulted in 11 reported eccentricity conditions. Outlet pressure and temperature field data were gathered for a subset of the FRAP measurement cases. Complete rake traverses were gathered at normalized eccentricities of $\varepsilon = 0\%, +30.9\%, +63.0\%$, and $+100\%$. Measurements using the rake sector traverses are presented based on corresponding local clearance at the FRAP to clarify their connection with the FRAP data. However, because the rakes traverse in various sectors of the annulus, they collect measurements over the entire range of local tip clearances. For this reason, the rake traverses are essential to understanding how the rotor-casing eccentricity is affecting the turbine performance around the annulus.

Efficiency Calculations. An integrated stage efficiency was initially calculated to understand how rotor-casing eccentricity affects overall turbine performance. Specifically, torque-based efficiency, η_Υ, and enthalpy-based efficiency, η_h, were calculated according to Eqs. (3) and (4), respectively

$$\eta_\Upsilon = \frac{\Upsilon\omega}{[\dot{m}_{\mathrm{MGP}} h_{\mathrm{MGP},1} + \dot{m}_c h_{c,1}] - [\dot{m}_{\mathrm{MGP}} h_{\mathrm{MGP},2s} + \dot{m}_c h_{c,2s}]} \tag{3}$$

Table 1 Estimated uncertainty of turbine measurements

Parameter	Total uncertainty
MGP flowrate, $\dot{m}_{\mathrm{MGP}}/\dot{m}_{\mathrm{MGP,ref}}$	±0.0040
Pressures, P/P_{ref}	±0.0010
Temperatures, T/T_{ref}	±0.0006
Normalized tip clearance, σ	±0.15
FRAP total pressure, $P_{\mathrm{tot}}/P_{\mathrm{dyn}}$	±0.020
FRAP static pressure, $P_{\mathrm{stat}}/P_{\mathrm{dyn}}$	±0.024
Flow yaw angle percentage $(\phi/\phi_{\mathrm{max}})$	±0.096

$$\eta_h = \frac{[\dot{m}_{MGP} h_{MGP,1} + \dot{m}_c h_{c,1}] - [(\dot{m}_{MGP} + \dot{m}_c) h_2]}{[\dot{m}_{MGP} h_{MPG,1} + \dot{m}_c h_{c,1}] - [\dot{m}_{MGP} h_{MGP,2s} + \dot{m}_c h_{c,2s}]} \quad (4)$$

A discussion on the effects of area-averaging and mass-averaging parameters was outlined by Cumpsty and Horlock [33]. For the present study, the efficiency formulations in Eqs. (3) and (4) were calculated using both area-averaged and mass-averaged enthalpy for comparison. These calculated efficiencies are given in the remainder of this paper in accordance with their respective operators. Through this comparison, potential efficiency differences due to redistributed flow in the tip regions were evaluated.

In this experiment, the conditions at the turbine outlet were spatially defined over an interval of time using the rake traverses. Although the pressure rake and temperature rake were separated instruments that measure different locations in time, the START facility is well-suited to performing these types of measurements due to its steady operating mode providing minimal temporal variations of operating conditions [34]. For the current tests, operating tolerances on inlet conditions were set to be 0.6 K and 0.7 kPa for temperature and pressure, respectively. However, as the separate pressure and temperature rakes were traversed across the measurement zones at the outlet, they defined the pressure and temperature at relative points in space at two distinct instances in time. To account for variations within the operating tolerances, the inlet parameters were averaged between these two times to minimize contributing errors.

Experimentally determined average profiles of temperature, total pressure, and static pressure were applied to spatially define the inlet parameters. An average static pressure profile was also applied at the outlet (based on the rotor exit three-hole probe measurements), which enabled the estimations of the turbine inlet and outlet velocity fields. Using these velocity fields and density information, Eqs. (3) and (4) were solved using either area- or mass-averaged quantities.

Efficiency Effects Due to Eccentricity

Using the definitions from Eqs. (3) and (4), the overall stage efficiencies are compared in Fig. 7 for a range of eccentricities. Range bars show a representative distribution of the precision for each of the two efficiency calculation techniques. Each type of efficiency is presented as a difference with respect to its corresponding concentric efficiency. The efficiencies show agreement to within uncertainty levels for three of the four efficiency calculations, which means that the interpretation of the trend to overall efficiency is largely independent of measurement type or averaging technique. Additionally, Fig. 7 shows that there is no clearly identifiable trend to the overall efficiency. This result indicates the validity of the assumption that the efficiency increase in the small clearance region is balanced by the efficiency decrease in the large clearance region, which results in a zero net change to overall stage efficiency. It is important to note that this result is based upon the tip gap range evaluated in this study.

This net zero efficiency change can be observed in greater detail by examining the radially averaged efficiency variation around the annulus using a mass-averaged efficiency. It is worth noting that the maximum difference of circumferential efficiency evaluated using mass averaging compared with that of area averaging was on the order of 0.2 points. Therefore, the trends to circumferential efficiency were consistent between the two averaging techniques. The agreement is likely because the tip leakage flow carries very little mass and also occupies a very small area, dictating that its effect on the circumferential efficiency is small regardless of the averaging technique applied. This result is consistent with Cumpsty and Horlock [33] who noted that spatial averaging is often reasonably consistent with other averaging, provided there is not a region of separated fluid in which a small mass flow is passed through a large area.

The radially mass-averaged efficiency is shown in Fig. 8, presented as a difference of efficiency with respect to the concentric case ($\varepsilon = 0$). It is worth noting that the raw radially averaged efficiency was smoothed using a moving window filter to remove the pitchwise efficiency variations caused by the upstream vanes and highlight the efficiency variations about the annulus specifically due to local tip clearance variation. These smoothed efficiency values are presented in Fig. 8. The gaps in the efficiency curves correspond to the inaccessible measurement regions shown in Fig. 5. These gaps are relatively small and do not inhibit the understanding of efficiency variations around the annulus. The locations of minimum and maximum clearance are labeled to highlight the anticipated regions of highest and lowest efficiency, respectively. As expected, the shape of the curves is similar to the clearance variation shown in Fig. 3, such that the amplitude of efficiency change increases with increasing eccentricity.

Notably, the circumferential extent of the low efficiency region is greater than the circumferential extent of the high efficiency region. There are a few potential explanations for why this behavior is observed. The spreading of the efficiency deficit could be associated with the mixing process that occurs as the flow moves downstream. As the flow exits the rotor, the increased strength of secondary flow features in a passage with a large tip clearance could create additional perturbations in the flow exiting a neighboring passage with a smaller clearance. Another explanation for the spreading of the low efficiency region could be that increased strength of secondary flow features in passages with increased tip clearance creates an effective flow area change that affects the flow of nearby passages. This type of flow interaction between passages is encountered in compressors during the onset of rotating stall when the tip leakage vortex creates a blockage which diverts the flow streamlines

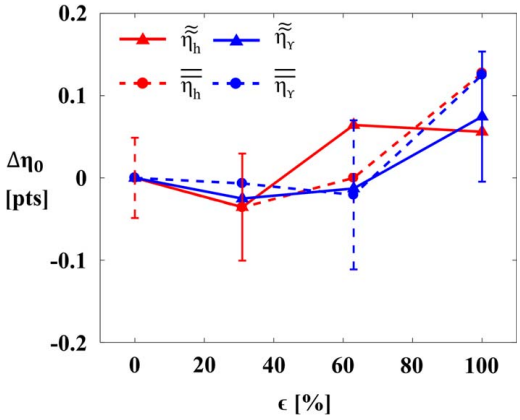

Fig. 7 Stage efficiency for different averaging techniques over a range of eccentricities

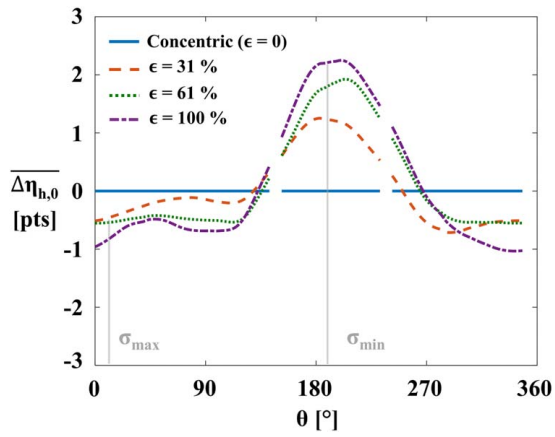

Fig. 8 Circumferential variation of efficiency for varying amounts of eccentricity

toward neighboring passages [35]. While additional studies are needed to understand the mechanisms driving the spread of the low efficiency region, it is likely that the maximum and minimum clearance regions are least affected because the spatial variation of tip clearance is minimized in those regions.

To understand how these efficiency variations compare with previous findings, the efficiency was plotted with respect to the local tip clearance in Fig. 9, along with a semi-empirical correlation [23]. The smoothed efficiency measurements corresponding to the most eccentric case are shown with markers at increments of 5 points to provide contrast from the correlation curve. The variation of the raw efficiency about the smoothed values is quantified by the shaded region, which shows the variation bounds corresponding to two standard deviations. The abscissa on the graph represents a normalized tip clearance value for the study with respect to the concentric case. The ordinate axis shows the change in efficiency from the concentric condition. The efficiency data in Fig. 8 are mapped from circumferential location to local tip clearance using the relationship shown in Fig. 3. Based on this relationship, two efficiency measurements exist for each localized tip clearance, excluding regions the rakes could not traverse as shown in Fig. 5. These two efficiency values were averaged together to effectively provide a functional relationship of efficiency versus tip clearance based on the eccentric performance.

The correlation presented in Fig. 9 by Lakshminarayana [23] was chosen due to its functional dependence on blade loading. Moreover, its derivation from fundamental physics makes it capable of predicting the efficiency deficit, and the corresponding effect on the flow field. The inputs for this correlation were obtained from an industry meanline turbine performance tool for the present geometry. In Fig. 9, the dashed portion of the correlation curve shows the extrapolation to tip clearances lower than those initially used in the derivation of the correlation [23].

The case with the greatest eccentricity is plotted in Fig. 9 because it covers the widest local tip clearance range. As noted previously in the discussion of Fig. 8, the circumferential extent of the low efficiency region is relatively large, which causes the measured efficiency change to be negative where the local clearance is equivalent to the concentric clearance ($\sigma = 0$). Interestingly, for small values of nondimensional clearance, σ, the data from each eccentricity test show a more severe relationship between efficiency and tip clearance than predicted by the correlation from Lakshminarayana [23]. Because the correlation is semi-empirical, it is possible that a lack of experimental data in the small clearance region is causing the diversion between the measurements and the correlation. Despite this behavior, Fig. 9 shows a reasonable prediction of the overall efficiency gradient, with good agreement occurring in the positive σ range. This agreement shows viability for tip clearance studies conducted using localized measurements based on eccentric rotor movements.

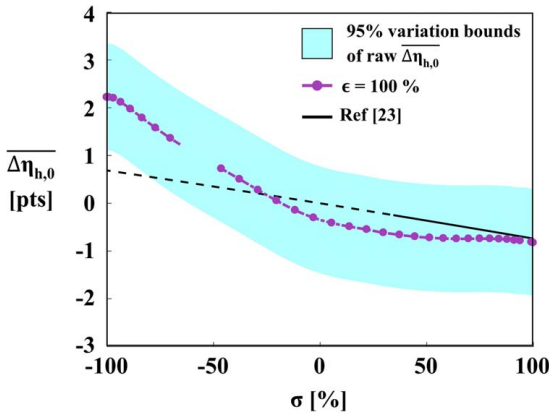

Fig. 9 Efficiency loss versus tip clearance trend comparison with correlation from Lakshminarayana

Rotor Exit Flow Field Measurements

Flow features exiting the turbine rotor were studied using a FRAP measurement system as previously discussed. Initially, the total pressure coefficient ($C_{p,\mathrm{tot}}$) and the absolute flow yaw angle (φ_{abs}) were examined in Fig. 10 for the concentric case to identify rotating flow structures and regions of secondary flow. At the FRAP measurement location, approximately 1.4 axial chord lengths downstream, diffusion of the blade wake and considerable mixing of the secondary flow features has occurred. However, the wake, which is characterized by low total pressure coefficient and flow underturning, is evident at the integer values of the rotor blade passage period (t/T). Between these wake regions are the passage regions, which are characterized by greater flow turning and higher total pressure coefficient.

To investigate the effects of local tip clearance variations on the rotor exit flow field, the circumferentially averaged, blade relative flow angle profiles were examined. Figure 11 shows these profiles as a difference with respect to their midspan values for four cases, which cover the entire range of studied eccentricities. As explained by Kaiser and Bindon [36], leakage flow traveling through the tip gap results in less flow deflection in the outer span region. This decreased deflection is shown in Fig. 11 in the

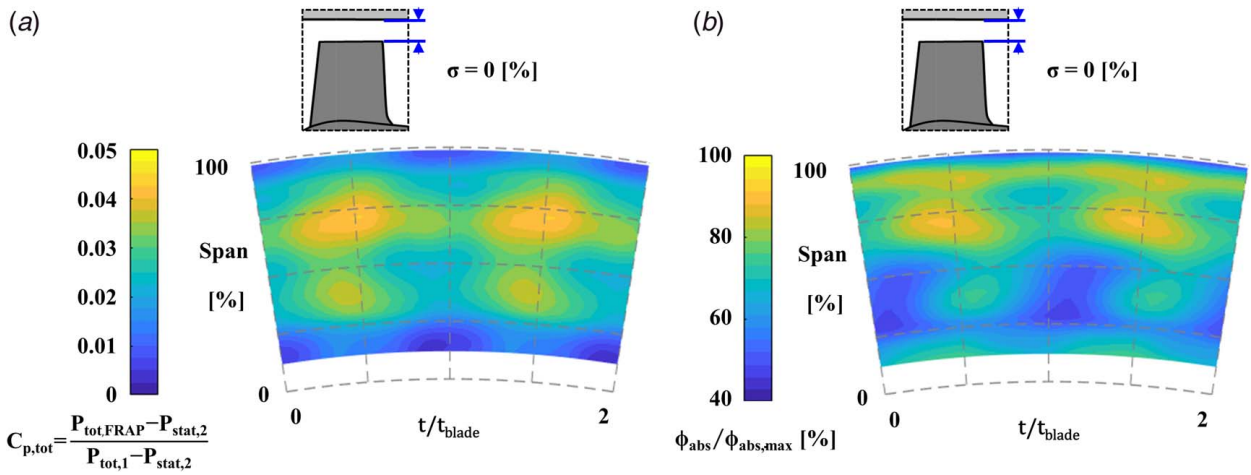

Fig. 10 Average blade passage contours of (*a*) total pressure coefficient ($C_{p,\mathrm{tot}}$) and (*b*) absolute flow angle for the concentric case

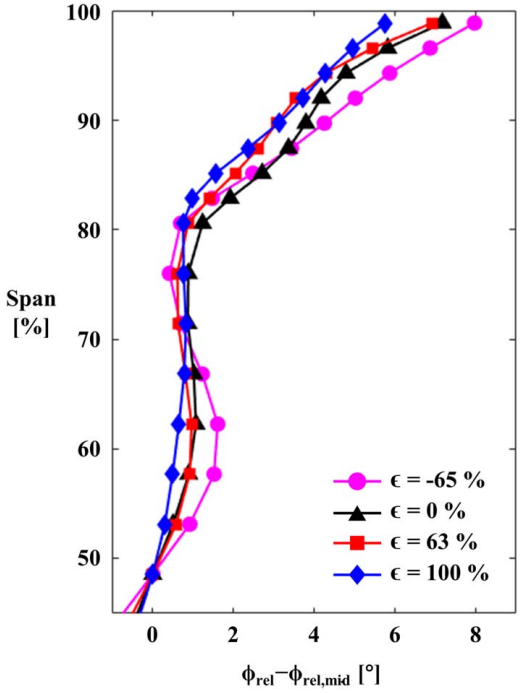

Fig. 11 Circumferentially averaged profiles of blade relative exit flow angle

region above 85% span, where ϕ_{rel} decreases (less turning) as the tip clearance increases. Notably, these relative flow angle changes in the outer span region are accompanied by flow angle variations at the other spanwise locations, which is likely the result of a slight flow redistribution. This redistribution likely explains the variations in the profile shape about the concentric profile. To gain a more quantitative understanding of the strength of the tip leakage flow and its variation with tip clearance, the SKE was investigated.

As the tip clearance is increased in the region of the FRAP, the leakage flowrate will increase as well. This additional leakage flow strengthens the secondary flows exiting the turbine rotor. Figure 12 shows the energy of the secondary flows for three eccentricity cases in the outer span region from 50% to 100% span. For each case, the secondary kinetic energy is given as a percentage of the total flow kinetic energy to isolate the changes to SKE specifically due to the local tip clearance variation. There is a general trend of increasing SKE/KE as tip clearances increase. This trend

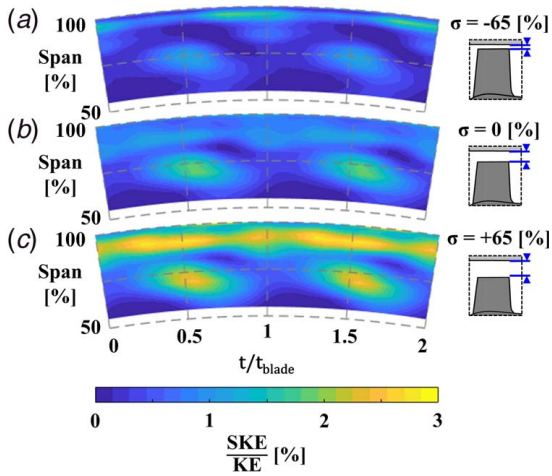

Fig. 12 Average rotor passage contours of SKE/KE in the outer 50% span for three local tip clearance cases

is most notable for locations above about 85% span, which is consistent with the region of decreasing deflection shown in Fig. 11.

Qualitatively, these contours show the relationship between the SKE of the leakage flow and the size of the tip gap. But, to gain a quantitative understanding of the relationship between these two parameters, the SKE was area averaged from 50% to 100% span for a complete ensemble-averaged rotor revolution as shown in Fig. 13. The outer 50% span region was chosen to capture the changes to both the TPV and the TLV. This averaging process results in a single SKE/KE value for each local clearance case.

To understand how the average SKE measurements compare with available correlations, a forced vortex model developed by Lakshminarayana [23] was evaluated at the FRAP measurement plane. The applicability of this model to the current study assumes that the increase in SKE must come from the increased energy of the TLV. Although there are other sources of SKE, these are assumed to be constant in the present analysis. The full details of the model are outlined in Ref. [23], but a brief description is given here for completeness.

First, the radius of the vortex (a) at the downstream measurement location is calculated empirically from Eq. (5) [37]

$$a = 0.14\left[\frac{d}{\tau}(C_L)^{0.5}\right]^{0.85} \tag{5}$$

where d is the longitudinal distance of the vortex from the leading edge, τ is the local tip clearance, and C_L is the lift coefficient. C_L was calculated as a function of the total pressure loss, flow velocity, inlet and outlet flow angles, density ratio, and blade row geometry [38] with inputs from a meanline prediction. Where possible, these parameters in the C_L computation were quantified in the rotor relative frame of reference because the analytical vortex model and its underlying equations were created for the cascade environment. Using the radius of the vortex, the angular rotation (ω) is computed through Eq. (6)

$$\omega = \frac{(1-K)\Gamma}{2\pi a^2} \tag{6}$$

where K is the fraction of lift retained at the tip and Γ is the vortex circulation. The vortex circulation was computed through two different methods [38] agreeing within 5%. Importantly, the current work deviates from the process outlined by Lakshminarayana [23] by calculating the fraction of lift retained at the tip from Eq. (7) [39]

$$K = e^{-\frac{14\tau}{C}} \tag{7}$$

where τ is the local tip clearance and C is the blade chord. This correlation was chosen because it is more applicable to the tip clearance

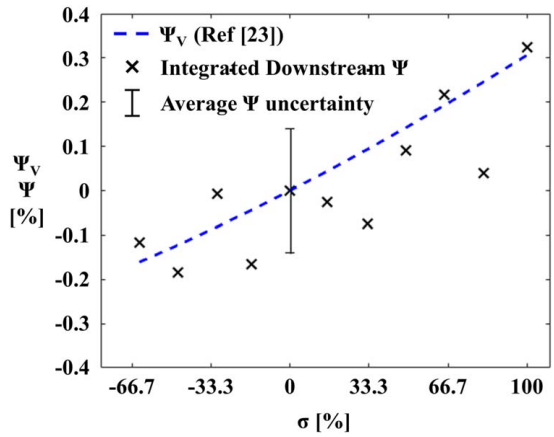

Fig. 13 Percent SKE trend with local tip clearance compared with forced vortex model

range of this study. The associated kinetic energy from the vortex (KE_V) is calculated using Eq. (8), by integrating the velocity over the area of the vortex

$$KE_V = \frac{\iint_0^{a,2\pi} 0.5\rho(\omega r)^2 r d\theta dr}{\pi a^2} = \frac{1}{4}\rho\omega^2 a^2 \tag{8}$$

where ρ is the density, (ωr) is the local velocity in the vortex, and a is the vortex radius. By evaluating the KE_V at multiple tip clearances, the change in the KE_V with respect to the concentric case can be found through Eq. (9)

$$\Delta KE_V = KE_V - KE_{V,0} \tag{9}$$

where $KE_V - KE_{V,0}$ is the change in kinetic energy with respect to the concentric case. To compare with experimental data, these results were normalized as a percent of the total kinetic energy through Eq. (10)

$$\Psi_V = \Delta KE_V / KE_{FRAP,Calc} \tag{10}$$

where KE_{FRAP} is the total kinetic energy at the FRAP measurement plane. KE_{FRAP} was calculated in the rotor relative frame of reference to be consistent with the calculation of C_L. Finally, the measured SKE/KE were computed with respect to the concentric case using Eq. (11).

$$\Psi = \left(\frac{SKE}{KE_{FRAP,meas}}\right) - \left(\frac{SKE_0}{KE_{FRAP,meas,0}}\right) \tag{11}$$

The trend to Ψ and Ψ_V is shown in Fig. 13. The experimental uncertainty of the FRAP measurement is also shown, which gives some context to the variations seen in the data. The uncertainty was computed by propagating the flow angle and Mach number root-sum-square uncertainty through the Ψ calculation. Note that the uncertainty is different for each case shown in Fig. 13, but only the average uncertainty across all cases is shown. The uncertainty across all cases is very uniform, with the maximum uncertainty varying from the average uncertainty by 0.023%.

As expected, there is an increase in SKE/KE as the tip clearance increases, which is correlated to an increase in KE_V. This agreement with the model indicates that the increase in measured SKE is primarily a result of increased energy of the TLV. Broadly, this result indicates that there is similarity in the flow exiting an eccentric rotor when compared with a concentric rotor with the same local tip clearance. This result further supports the potential to conduct tip clearance studies using local measurements gathered about local clearance changes.

Summary and Conclusions

This paper studied the effects of rotor-casing eccentricity on the efficiency of a one-stage continuous-operation test turbine operating with true engine hardware at engine-relevant conditions. This study was made possible through the use of a magnetic levitation bearing system that was used to precisely position the rotor over a wide range of rotor-casing eccentricities.

Circumferential traverses of total pressure and total temperature rakes provided the turbine exit flow conditions to characterize efficiency in multiple sectors covering the majority of the annulus. No identifiable trend was observed to overall stage efficiency with increasing eccentricity. The circumferential variation of efficiency indicated increased efficiency in the small clearance region was balanced by the decreased efficiency in the large clearance region over the range of tip gap sizes studied. When examining the relationship between local efficiency and local clearance, the overall efficiency gradient was reasonably predicted by a semi-empirical correlation. This collection of efficiency results also showed a widening of the circumferential extent of the low efficiency region. Further study is needed to identify the mechanisms driving this behavior.

To support the eccentric efficiency measurements, a fast-response aerodynamic probe (FRAP) was positioned downstream of the rotor to observe the loss generating flow structures as they propagate downstream with changing local blade tip clearances. For the concentric case, the absolute flow yaw angle and total pressure coefficient were used to locate the approximate locations of the wake and passage flows. Circumferentially averaged profiles of blade relative flow angle showed the expected trend of decreased turning in the outer span region as tip clearance increased. Furthermore, a relationship between secondary kinetic energy and local tip clearance was observed by integrating over the outer 50% span at the FRAP measurement plane. This trend showed good agreement with a semi-empirical forced vortex model that approximates the energy in the tip leakage vortex. Overall, these flow field measurements help explain the stage efficiency results and may also be important to the performance of downstream turbine stages.

This agreement points to the utility of eccentric rotor studies as a viable approach for quantifying local tip clearance effects with isolated sensors. Because the effects of the localized clearance are highly similar to a concentric rotor and casing with an equivalent uniform clearance, rapid iterations of tip clearance variations and wide ranges of tip clearance changes can be assessed with minimal required test time and without the need for costly hardware changes.

The implications of these results can be applied to both the design process and maintenance cycles of gas turbine engines. With accelerated test timescales and reduced costs, researchers have an ability to build more complete datasets, and engine manufacturers can make more confident design decisions. Further, this type of testing can be applied to understand how the performance of gas turbine engines varies over time as faults that cause non-axisymmetric tip clearances occur, which is necessary to deciding when an engine needs part replacements or repair.

Acknowledgment

The authors would like to recognize and thank Pratt & Whitney for supporting research presented in this paper. Specific thanks go to Jin Hu from Pratt & Whitney for computational predictions and technical feedback. This material is based upon work supported by the Department of Energy under Award Number DE-FE0031288. This report was prepared as an account of work sponsored by an agency of the United States Government. Neither the United States Government nor any agency thereof, nor any of their employees, makes any warranty, express, or implied, or assumes any legal liability or responsibility for the accuracy, completeness, or usefulness of any information, apparatus, product, or process disclosed, or represents that its use would not infringe privately owned rights. Reference herein to any specific commercial product, process, or service by trade name, trademark, manufacturer, or otherwise does not necessarily constitute or imply its endorsement, recommendation, or favoring by the United States Government or any agency thereof. The views and opinions of authors expressed herein do not necessarily state or reflect those of the United States Government or any agency thereof.

Conflict of Interest

There are no conflicts of interest.

Data Availability Statement

The authors attest that all data for this study are included in the paper.

Nomenclature

a = radius of vortex core
d = distance downstream from blade leading edge

h = enthalpy
r = radius
t = time
C = blade chord
K = fraction of lift retained at the tip
P = pressure
T = temperature
V = velocity
$\dot{m}$ = mass flowrate
t_{blade} = blade passing period
C_L = lift coefficient based on mean velocity
$C_{P,\text{tot}}$ = pressure coefficient $= (P_{\text{tot,FRAP}} - P_{\text{stat},2})/(P_{\text{tot},1} - P_{\text{stat},2})$
C_x = blade axial chord
KE = kinetic energy $= \frac{1}{2}\rho V^2$
SKE = secondary flow kinetic energy $= \frac{1}{2}\rho V_{\text{sec}}^2$

Greek Symbols

Γ = vortex circulation
Δ = change in quantity
ε = normalized eccentricity
η = efficiency
θ = circumferential angle
ρ = *density*
σ = normalized tip clearance $= (\tau - \tau_0)/(\tau\text{max} - \tau_0)$
τ = tip clearance
Υ = torque
ϕ = flow yaw angle
Ψ = SKE/KE change with respect to the concentric case
ω = angular velocity

Subscripts

0 = total quantity, with respect to concentric
1 = measurement at turbine inlet (P1)
2 = measurement at turbine exit (P2)
abs = absolute frame of reference
c = coolant
dyn = dynamic quantity
FRAP = plane of FRAP
max = maximum quantity across all cases
mid = midspan
ref = reference measurement
rel = blade relative frame of reference
s = isentropic
sec = relating to the secondary flow
stat = static quantity
tot = total quantity
v = vortex
x = x component of movement
y = y component of movement

Operators

$\bar{Q}$ = mass average in r-direction
$\overline{\overline{Q}}$ = mass average in r-θ plane
$\tilde{Q}$ = spatial average in r-direction
$\tilde{\tilde{Q}}$ = spatial average in r-θ plane

References

[1] Gupta, A., and Bais, A. S., 2018, "Global Market Insights, Gas Turbine Market Growth Statistics," Global Projections Report No. 2024.
[2] Global Data PLC, 2018, "The Global Commercial Aircraft Market 2018–2028," Report No. GD-DF0151SR.
[3] Bunker, R. S., 2006, "Axial Turbine Blade Tips: Function, Design, and Durability," J. Propuls. Power, **22**(2), pp. 271–285.
[4] Lattime, S. B., and Steinetz, B. M., 2002, "Turbine Engine Clearance Control Systems: Current Practices and Future Directions," 38th AIAA/ASME/SAE/ASEE Joint Propulsion Conference & Exhibit, Indianapolis, IN, July 7–10, p. 3790. AIAA 2002-3790.
[5] Alford, J. S., 1965, "Protecting Turbomachinery From Self-Excited Rotor Whirl," J. Eng. Power, **87**(4), pp. 333–343.
[6] Vance, J. M., and Laudadio, F. J., 1984, "Experimental Measurement of Alford's Force in Axial Flow Turbomachinery," ASME J. Eng. Gas Turbines Power, **106**(3), pp. 585–590.
[7] Martinez-Sanches, M., Jaroux, B., Song, S. J., and Yoo, S., 1995, "Measurement of Turbine Blade-Tip Rotordynamic Excitation Forces," ASME J. Turbomach., **117**, pp. 384–392.
[8] Song, S. J., and Martinez-Sanchez, M., 1997, "Rotordynamic Forces Due to Turbine Tip Leakage: Part I-Blade Scale Effects," ASME J. Turbomach., **119**(4), pp. 695–703.
[9] Song, S. J., and Martinez-Sanchez, M., 1997, "Rotordynamic Forces Due to Turbine Tip Leakage: Part II-Radius Scale Effects and Experimental Verification," ASME J. Turbomach., **119**(4), pp. 704–713.
[10] Guo, Z., Rhode, D. L., and Davis, F. M., 1994, "Computed Eccentricity Effects on Turbine rim Seals at Engine Conditions with a Mainstream," Turbo Expo: Power for Land, Sea, and Air, Vol. 78835, p. V001T01A007, American Society of Mechanical Engineers. 94-GT-31.
[11] Guo, Z., and Rhode, D. L., 1999, "Predicted Combined Effects of Purge Flow and Rotor-Casing Eccentricity on Ingress Heating," J. Propuls. Power, **15**(3), pp. 454–461.
[12] Bindon, J. P., 1989, "The Measurement and Formation of Tip Clearance Loss," ASME J. Turbomach., **111**(3), pp. 257–263.
[13] Peters, D. W., and Moore, J., 1995, "Tip Leakage Loss Development in a Linear Turbine Cascade," AGARD-CP-571, pp.12-1–12-13.
[14] Yaras, M., Yingkang, Z., and Sjolander, S. A., 1989, "Flow Field in the Tip Gap of a Planar Cascade of Turbine Blade," ASME J. Turbomach., **111**(3), pp. 276–283.
[15] Sjolander, S. A., 1997, "Modelling of Tip-Clearance Flow in Axial Turbines," VKI Lecture Series: Secondary and Tip-Clearance Flows in Axial Turbines, pp. 1–32.
[16] Morphis, G., and Bindon, J. P., 1994, "The Performance of a Low Speed One and a Half Stage Axial Turbine With Varying Rotor Tip Clearance and Tip Gap Geometry," International Gas Turbine and Aeroengine Congress and Exposition, The Hague, Netherlands, June 13–16, p. V001T01A152, American Society of Mechanical Engineers, 94-GT-481.
[17] Yoon, S., Curtis, E., Denton, J., and Longley, J., 2014, "The Effect of Clearance on Shrouded and Unshrouded Turbines at Two Levels of Reaction," ASME J. Turbomach., **136**(2), p. 021013.
[18] Hong, Y. S., and Groh, F. G., 1966, Axial Turbine Loss Analysis and Efficiency Prediction Method, p. 112.
[19] Ameri, A. A., Steinthorsson, E., and Rigby, D. L., 1999, "Effects of Tip Clearance and Casing Recess on Heat Transfer and Stage Efficiency in Axial Turbines," ASME J. Turbomach., **121**(4), pp. 683–693.
[20] Kofsky, M. G., 1961, "Experimental Investigation of Three Tip-Clearance Configurations Over a Range of Tip Clearance Using a Single-Stage Turbine of High Hub-to-Tip Radius Ratio," NASA TM X-472.
[21] Marshall, R., and Rogo, C., 1968, "Experimental Investigation of Low Aspect Ratio and Tip Clearance on Turbine Performance and Aerodynamic Design," Usaavlabs Technical Report 67-80.
[22] Szanca, E. M., Schum, H. J., and Hotz, G. M., 1974, "Research Turbine for High Temperature Core Engine Application II—Effect of Rotor Tip Clearance on Overall Performance," NASA TN D-7557.
[23] Lakshminarayana, B., 1970, "Methods of Predicting the Tip Clearance Effects in Axial Flow Turbomachinery," ASME J. Basic Eng., **92**(3), pp. 467–480.
[24] Craig, H. R. M., and Cox, H. J. A., 1970, "Performance Estimation of Axial Flow Turbines," Proc. Inst. Mech. Eng., **185**(1), pp. 407–424.
[25] Booth, T. C., 1985, "Importance of Tip Clearance Flows in Turbine Design," Tip Clearance Effects in Axial Turbomachines, VKI Lecture Series, pp. 1–15.
[26] Gaetani, P., Persico, G., Dossena, V., and Osnaghi, C., 2007, "Investigation of the Flow Field in a High-Pressure Turbine Stage for Two Stator-Rotor Axial Gaps—Part II: Unsteady Flow Field," ASME J. Turbomach., **129**(3), pp. 580–590.
[27] Behr, T., Kalfas, A. I., and Abhari, R. S., 2008, "Control of Rotor Tip Leakage Through Cooling Injection From the Casing in a High-Work Turbine," ASME J. Turbomach., **130**(3), p. 031014.
[28] Barringer, M. D., Coward, A., Clark, K. P., Thole, K. A., Schmitz, J., Wagner, J., Alvin, M. A., Burke, P., and Dennis, R. "The Design of a Steady Aero Thermal Research Turbine (START) for Studying Secondary Flow Leakages and Airfoil Heat Transfer," GT2014-25570.
[29] Berdanier, R. A., DeShong, E., Thole, K. A., and Robak, C., 2021, "Evaluating the Effects of Transient Purge Flow on Stator-Rotor Seal Performance," ASME J. Turbomach., **143**(2), p. 021006.
[30] Pfau, A., Schlienger, J., Kalfas, A. I., and Abhari, R. S., 2003, "Unsteady, 3-Dimensional Flow Measurement Using a Miniature Virtual 4 Sensor Fast Response Aerodynamic Probe (FRAP)," Proceedings of ASME Turbo Expo 2003, Atlanta, GA, June 16–19, Vol. 36843, pp. 307–315, Paper No. GT2003-38128.
[31] Kupferschmied, P., Köppel, P., Gizzi, W., Roduner, C., and Gyarmathy, G., 2000, "Time-Resolved Flow Measurements With Fast-Response Aerodynamic Probes in Turbomachines," Meas. Sci. Technol., **11**(7), pp. 1036–1054.
[32] Figliola, R. S., and Beasley, D. E., 2014, *Theory and Design for Mechanical Measurements*, John Wiley & Sons, New York.

[33] Cumpsty, N. A., and Horlock, J. H., 2006, "Averaging Nonuniform Flow for a Purpose," ASME J. Turbomach., **128**(1), pp. 120–129.
[34] Clark, K., Barringer, M., Johnson, D., Thole, K., Grover, E., and Robak, C., 2018, "Effects of Purge Flow Configuration on Sealing Effectiveness in a Rotor-Stator Cavity," ASME J. Eng. Gas Turbines Power, **140**(11), p. 112502.
[35] Day, I. J., 1993, "Active Suppression of Rotating Stall and Surge in Axial Compressors," ASME J. Turbomach., **115**(1), pp. 40–47.
[36] Kaiser, I., and Bindon, J. P., 1997, "The Effect of Tip Clearance on the Development of Loss Behind a Rotor and a Subsequent Nozzle," International Gas Turbine & Aeroengine Congress & Exhibition, Orlando, FL, June 2–5, Vol. 78682, p. V001T03A011, American Society of Mechanical Engineers, Paper No. 97-GT-53.
[37] Rains, D. A., 1954, "Tip Clearance Flows in Axial Flow Compressors and Pumps," Report No. 5.
[38] Lakshminarayana, B., 1995, *Fluid Dynamics and Heat Transfer of Turbomachinery*, John Wiley & Sons, New York.
[39] Lewis, R. I., and Yeung, E. H. C., 1977, "Vortex Shedding Mechanisms in Relation to Tip Clearance Flows and Losses in Axial Flow Fans," Aeronautical Research Council, R&M No. 3829.